J Therm Anal Calorim (2015) 119:1415–1428
DOI 10.1007/s10973-014-4292-3

Comparison of vibrational dynamics, thermal behaviour, and phase transition in $[Ni(NH_3)_4](ReO_4)_2$ and $[Ni(NH_3)_6](ReO_4)_2$

Łukasz Hetmańczyk · Joanna Hetmańczyk

Received: 9 June 2014 / Accepted: 4 November 2014 / Published online: 3 December 2014

Abstract The differences between thermal and vibrational properties of $[Ni(NH_3)_4](ReO_4)_2$ and $[Ni(NH_3)_6](ReO_4)_2$ are reported. The differential scanning calorimetry revealed that tetraamminenickel(II) perrhenate exhibits, in the temperature range of 300–140 K, one phase transition at ca. $T_c^h = 188$ K (on heating) and $T_c^c = 185$ K (on cooling). In the case of hexaamminenickel(II) perrhenate, no phase transition was observed in the same temperature region. Thermogravimetric measurements showed that the decomposition proceeds in the two main stages. In the first stage, a complete deammination takes place and next Re_2O_7 is released. TG measurements showed that NH_3 molecules are not equivalently bonded to central atom. The final and intermediate products of decomposition were analysed by means of infrared spectroscopy. The final product of thermal decomposition of both compounds is nickel(II) oxide. The analysis of far infrared spectra revealed that anions in $[Ni(NH_3)_6](ReO_4)_2$ have disturbed tetrahedral symmetry, whereas in $[Ni(NH_3)_4](ReO_4)_2$ they seem to form polymeric chains. The variation of the activation energies of the deammination and decomposition steps of $[Ni(NH_3)_6](ReO_4)_2$ was calculated through the model-free isoconversional Kissinger–Akahira–Sunose method and model-free Kissinger method. Infrared spectra were calculated by the DFT method and quite a good agreement with the experimental data was obtained.

Ł. Hetmańczyk · J. Hetmańczyk
Frank Laboratory of Neutron Physics, Joint Institute for Nuclear Research, 141980 Dubna, Russian Federation

Ł. Hetmańczyk (✉) · J. Hetmańczyk
Department of Chemical Physics, Faculty of Chemistry, Jagiellonian University, ul. Ingardena 3, 30-060 Cracow, Poland
e-mail: lukasz.hetmanczyk@uj.edu.pl; hetmancz@chemia.uj.edu.pl

Keywords Hexaamminenickel(II) perrhenate · Tetraamminenickel(II) perrhenate · Phase transition · Thermal decomposition · TG · Infrared spectroscopy · DSC

Introduction

Compounds of the type: $[M(NH_3)_x](ReO_4)_2$ ($x = 4, 6$) are particularly interesting molecular materials because of the occurrence of different reorientational motions of the complex cations $[M(NH_3)_x]^{2+}$, NH_3 ligands, and tetrahedral ReO_4^- anions. The various hexaamminenickel(II) complexes with different anions as a counter ion were intensively examined up to now. Here we will focus only on compounds containing tetrahedral anions with one negative charge. Phase polymorphism of compounds with ClO_4^- and BF_4^- anions and $[Ni(NH_3)_6]^{2+}$ cation was intensively investigated over past four decades [1, 2]. At room temperature they crystallize in a cubic system, space group No. 225, Fm-3 m, with four molecules per unit cell. Two phase transitions were found in each complex: one so called large and the second so called small. In case of $[Ni(NH_3)_6](ClO_4)_2$, the large anomaly was found at ca. 173 K and the small and diffused at ca. 143 K. The phase transition temperatures for $[Ni(NH_3)_6](BF_4)_2$ equal to 140.1 K (large, sharp) and ca. 110 K (small, diffused). It is interesting to extend similar investigations also to the family of compounds containing tetrahedral perrhenate anion with one negative charge. Unfortunately, the literature concerning basic properties of the title compounds is rather limited. The decomposition of $[Ni(NH_3)_4](ReO_4)_2$ was investigated by Chakravorti et al. [3] by the TG method but only up to 573 K. The authors have found that complete deammination of this compounds proceeds in two stages. According to these authors, the electronic spectra

indicate that $[Ni(NH_3)_4]^{2+}$ ion is tetragonal. On the other hand, the magnetic measurements indicate that Ni^{2+} complex is six-coordinate [3]. We have found none TG data for $[Ni(NH_3)_6](ReO_4)_2$. Thus, one of the aims of this work is to fill in this gap as well as extend knowledge about their thermal properties in the wide temperature range and to make a comparison between them. The low temperature phase transition in tetraamminenickel(II) perrhenate is reported in our paper for the first time. We have also tried to get answer about final and intermediate products of decompositions using infrared spectroscopy. Most of the investigated $[Ni(NH_3)_6]X_2$ compounds ($X = Cl^-$, Br^-, ClO_4^-, BF_4^-, and NO_3^-) is chemically stable even exposed on air. The hexaamminenickel(II) perrhenate is unstable and slowly transforms to tetraamminenickel(II) perrhenate. Change of sample color from violet to blue accompanies this process.

The second goal of this project is to compare infrared spectra and give its interpretation for both substances. The far infrared data for the $[Ni(NH_3)_6](ReO_4)_2$ compound were registered and discussed for the first time. The third aim of our paper is to shed a light on activation energies connected with particular steps of decomposition. To achieve this goal, we have used Kissinger–Akahira–Sunose (KAS) model-free approach [4] and Kissinger method [5, 6]. This novel approach has recently been growing in popularity and is generally used to study the kinetics of solid-state reactions. This method allows the estimation of activation energy without choosing a reaction model and reaction order. Kinetic studies on the thermal deammination reactions of hexaamminenickel(II) compounds are reported in the literature [7]. The activation energies of the deammination were calculated using isoconversional methods and indicate that this process has a multi-step nature.

Experimental

The hexaamminenickel(II) perrhenate was obtained in the manner described in [8, 9]. The nickel(II) carbonate basic hydrate (1 g, $NiCO_3{\cdot}2Ni(OH)_2{\cdot}xH_2O$) purchased from Sigma-Aldrich Company was dissolved in perrhenic acid (5 g, 75–80 mass% in H_2O, from Sigma Aldrich). The mixture was heated and filtered out in order to get rid of excess of not reacted nickel(II) carbonate. Next NH_{3aq} was added drop wise to the filtered greenish solution. The color changed to violet. Finally, this mixture was cooled to ca. −10 °C. The precipitated needle-shaped violet crystals were filtered out and dried. The obtained $[Ni(NH_3)_6](ReO_4)_2$ is unstable on air and transforms to blue $[Ni(NH_3)_4](ReO_4)_2$ within several minutes. However, when it is kept closed (preferably under NH_3 vapor) such decomposition is not observed and hexaamminenickel(II) perrhenate is stable and can be stored for a long period.

The contents of nitrogen and hydrogen in the $[Ni(NH_3)_4](ReO_4)_2$ were determined using elemental analysis on a EURO EA 3000 apparatus. Theoretical contents: N, 8.93 %; H, 1.93 %. Found: N, 8.90 %; H, 1.82 %. The elemental analysis of the title compound confirmed the presence of the stoichiometric number of four NH_3 molecules in the complex cation.

The thermogravimetric analyses (TG) with simultaneous differential thermal analyses (SDTA) measurements were performed using a *Mettler-Toledo 851*^{e} apparatus. Consecutive, samples of masses equal to 26.2094 mg of $[Ni(NH_3)_6](ReO_4)_2$ and 28.9680 mg of $[Ni(NH_3)_4](ReO_4)_2$ were placed in 150 µl platinum crucibles. The measurements were made in a flow of Argon (60 cm^3 min^{-1}), within temperature range of 295–1,275 K. The TG measurements were performed at a constant heating rate of 10 K min^{-1}. The simultaneous evolved gas analysis (EGA) was performed during the experiments by a joined on-line quadruple mass spectrometer (TG-MS) using a *Thermostar-Balzers* apparatus. The temperature was measured by a Pt–Pt/Rh thermocouple with an accuracy of ±0.5 K. In order to estimate the energy activation for identified decomposition steps further TG runs (with the same conditions but without MS signals) for $[Ni(NH_3)_6](ReO_4)_2$ were performed with the heating rates: 5, 7.5 and 15 K min^{-1}. The following initial sample masses were used 28.3826, 20.4543, and 26.1700 mg, respectively.

The DSC measurements were performed on heating (temperature range 140–300 K) and cooling (temperature range 300–140 K) using a *Mettler-Toledo 822*^{e} calorimeter. The samples of masses equal to 22.67 mg (18.02 mg second run) for $[Ni(NH_3)_4](ReO_4)_2$ and 9.64 mg for $[Ni(NH_3)_6](ReO_4)_2$ were placed in 40 µl aluminum partially open crucibles (micro hole preserves constant pressure over the sample). Measurements were performed under constant flow of Argon (80 cm^3 min^{-1}) with the heating/cooling rate being equal to 10 K min^{-1}. Additionally, for sample of mass equal to 18.02 mg second DSC run with scanning rate being equal to 20 K min^{-1} was performed.

The enthalpy change (ΔH) was calculated by numerical integration of the DSC curve under the anomaly peak after a linear background arbitrary subtraction. The entropy change (ΔS) was calculated using the formula $\Delta S = \Delta H / T_c$. For sharp peaks, the values were calculated to a high accuracy (4 %), whereas for the diffuse peak they were estimated only.

Fourier transforms far and middle infrared (FT-FIR and FT-MIR) absorption measurements were performed using a *Bruker Vertex 70v* vacuum Fourier Transform spectrometer. The transmission spectra were collected with a resolution of 2 cm^{-1} and with 32 scans per each spectrum. The

FT-FIR spectra (500–50 cm^{-1}) were collected for sample suspended in Apiezon N grease and placed on polyethylene (PE) disk. The FT-MIR spectra (4,000–500 cm^{-1}) were collected for sample in a KBr pellet.

Results and discussion

Spectroscopic identification of samples and vibrational analysis

Figure 1 presents a comparison of FT-MIR (4,000–500 cm^{-1}) and FT-FIR (500–30 cm^{-1}) spectra registered for $[Ni(NH_3)_6](ReO_4)_2$ (Fig. 1a, violet curve) and $[Ni(NH_3)_4](ReO_4)_2$ (Fig. 1b, blue curve) with calculated spectra. The vertical line visible in Fig. 1 separates far from middle infrared region. The MIR spectra registered for both compounds are very similar to each other. Moreover, they are typical for members of the ammine complexes group [10–12]. Only one subtle difference between $[Ni(NH_3)_6](ReO_4)_2$ and $[Ni(NH_3)_4](ReO_4)_2$ can be noticed. In the latter case, a weak additional band at 1,411 cm^{-1} is observed which allows one to distinguish between the two title compounds. The IR data obtained for $[Ni(NH_3)_4](ReO_4)_2$ in the 4,000–250 cm^{-1} wavenumber region were presented in paper [3]. Infrared spectrum (MIR and FIR) registered by us in the 4,000–30 cm^{-1} wavenumber region is in good agreement with data presented by Chakravorti et al. [3]. However, our data revealed more details probably due to better resolution used. The band registered at 1,411 cm^{-1} is rather weak, whereas in paper [3] this band (1,400 cm^{-1}) was denoted as very strong (vs). Moreover, we were able to register five bands in the 1,345–1,100 cm^{-1} region instead of only one. The splitting of $\rho(NH_3)$ at ca. 680 cm^{-1} is also observed in our case. Two additional bands are visible as shoulders at 645 and 580 cm^{-1}. Since we were able to measure FIR spectrum down to 30 cm^{-1} five additional bands (219, 207, 150, 114, 92 cm^{-1}) were revealed. Splitting of some bands suggests symmetry lowering of the ideal tetrahedral arrangement of anions and cations. Middle infrared spectrum obtained by us for $[Ni(NH_3)_6](ReO_4)_2$ is in a very good agreement with data reported by Müller et al. [13]. However, splitting of the bands at ca. 1,200 and 680 cm^{-1} is clearly visible. This suggests that octahedral and tetrahedral symmetry of particular cation is broken. According to Nakamoto [10] the ReO_4^- has the following normal modes: fully symmetric stretching $\nu_1(A_1) =$ 971 cm^{-1}, double degenerated $\nu_2(E) = 331$ cm^{-1}, triply degenerated $\nu_3(F_2) = 920$ cm^{-1} and $\nu_4(F_2) = 331$ cm^{-1}. All four vibrations are Raman active, but only ν_3 and ν_4 are IR active. However, in the case of both discussed compounds the tetrahedral symmetry of the anion is disturbed. The distortion led to the situation that formally forbidden (by selection rules) modes are also allowed in the infrared measurements. As a result splitting of ν_4 at ca. 920 cm^{-1} is observed. The lowering of the anion symmetry is also responsible for becoming active a fully symmetric Re–O stretching (breathing vibrations) at ca. 966 cm^{-1}. Splitting of the bands connected with anion internal vibrations is even better visible in the far infrared region. The ν_2 mode is no longer silent. Moreover, splitting of this band appears. The far infrared spectrum obtained for $[Ni(NH_3)_6](ReO_4)_2$ indicates that in the solid-state cations and anions are distorted. In the case of $[Ni(NH_3)_4](ReO_4)_2$ the situation is slightly different. The careful inspection of the FIR spectrum registered for this compound revealed additional bands at 219 (shoulder at 207), 150, 114 and 92 cm^{-1}. Their positions agree well with bands registered for Re_2O_7 in Raman scattering measurements (see Table 4). The more detailed discussion concerning crystal structure and infrared spectrum of dirheniumheptaoxide can be found in [14]. Here we can conclude that FIR spectrum obtained for $[Ni(NH_3)_4](ReO_4)_2$ can be interpreted as evidence that in the crystal structure

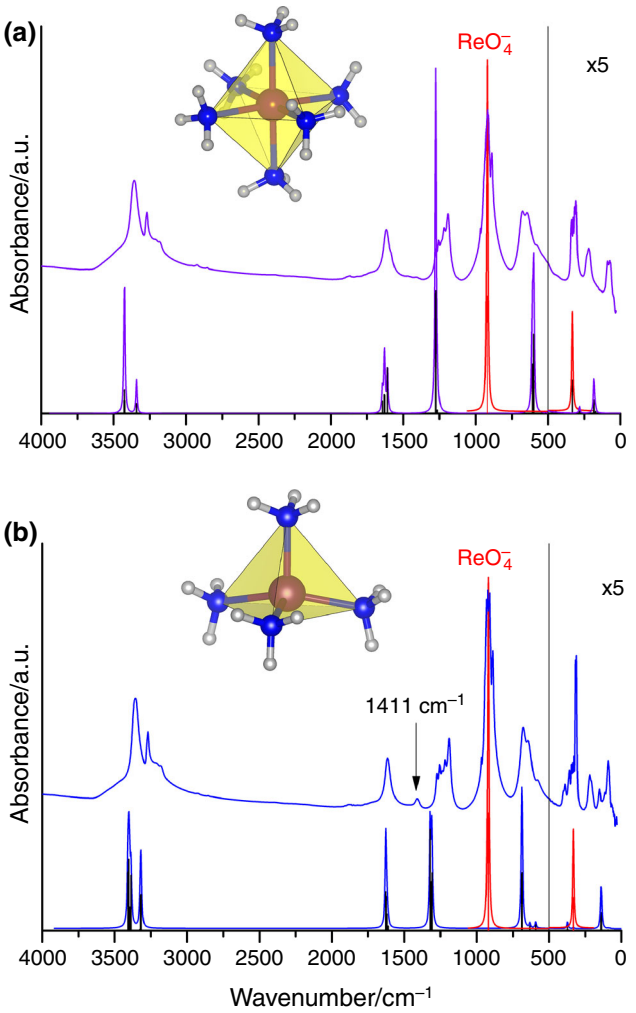

Fig. 1 Comparison of the experimental IR with calculated spectra for isolated molecules $[Ni(NH_3)_6]^{2+}$, $[Ni(NH_3)_4]^{2+}$ and ReO_4^-

ReO_4 units do not exist as a separate tetrahedrons but rather are joined together through complex cations to form long polymeric chain. The formation of Ni–O–Re bond is probably responsible for band at 219 cm^{-1}.

In order to support interpretation of experimental data (especially in the FIR wavenumber region), the calculations of infrared frequencies and intensities were performed. Theoretical IR spectra were calculated separately for an isolated perrhenic anion and isolated complex cation using Gaussian09 package [15] installed on ZEUS supercomputer in Academic Computer Center Cyfronet AGH in Cracow. The calculation were performed using well know and widely used B3LYP functional [16, 17]. The 6-311 + G(d,p) basis were set on N, O, H atoms, whereas Lanl2DZ and Lanl2TZ basis set were used for Ni and Re, respectively [18, 19]. The tetrahedral symmetry was assumed for ReO_4^-. In case of complex cation the octahedral and tetrahedral symmetry was employed for $[Ni(NH_3)_6]^{2+}$ and $[Ni(NH_3)_4]^{2+}$, respectively. Of course the forth coordination cation can take a square symmetry also. However, this symmetry is less popular for nickel-containing compounds. We have performed calculation also for a square symmetry of tetraaminenickel(II). One imaginary frequency was obtained in this case and the molecule (linear N–Ni–N bond) was bent after geometry optimization. We were not able to get rid of this imaginary frequency even by rotation of NH_3 molecules. This suggests that square symmetry can be treated as a transition state and tetrahedral arrangement is preferred and stable. The theoretical spectra calculated for complex cations and shown in Fig. 1ab were scaled by factor 0.9688 [20]. The results obtained for ReO_4^- (presented in Fig. 1 as a red line) were not scaled because they agree well with experimental ones. The following wavenumbers were obtained for anion: $\nu_1 = 982\ cm^{-1}$, $\nu_2 = 332\ cm^{-1}$, $\nu_3 = 920\ cm^{-1}$, $\nu_4 = 332\ cm^{-1}$. The obtained intensities (delta Dirac) were convoluted with Lorentzian (FWHM = 20 cm^{-1}) line shape. The overall good match between calculated and experimental IR spectra is observed despite the simplicity of assumed model. All the bands presented in IR spectrum are predicted by calculation. Since FIR and MIR spectra were measured in two experiments, the experimental intensities in both regions were scaled independently. For better readability the intensities in FIR region (calculated and experimental) were magnified by factor 5. Bands position, relative intensities and their assignments are gathered in Table 1. Interpretation was done taking into account data presented in paper [3, 10, 13] and quantum chemical calculations (QC) described above. The analysis of normal modes was supported by visualization of particular vibrations.

Thermal decomposition

Figure 2 shows comparison of thermal decomposition for both compounds. The violet and blue colors were used for $[Ni(NH_3)_6](ReO_4)_2$ and $[Ni(NH_3)_4](ReO_4)_2$, respectively. The TG, DTG, MS and SDTA curves were recorded at a constant heating rate of 10 K min^{-1} in the temperature range of 300–1,275 K. During the TG experiment, the following, selected MS line were registered *m/e*: 14, 16, 17, 18, 28, 30, 32, 44, 46 but only lines representing NH_3 showed some signal, and thus only $m/e = 17$ is shown. Decomposition process can be divided into two main stages. In the first stage both compounds lost all NH_3 ligands up to ca. 600 K. In case of $[Ni(NH_3)_6](ReO_4)_2$ all the ammonia ligands are released in three sub-steps ($2NH_3 + 2NH_3 + 2NH_3$), whereas two sub-steps ($2NH_3 + 2NH_3$) are observed for $[Ni(NH_3)_4](ReO_4)_2$. This behaviour suggests firstly that some kind of non-equivalency of NH_3 groups exists and secondly that two out of six ligands in $[Ni(NH_3)_6](ReO_4)_2$ are considerably weaker bounded to central atom and are released in temperatures just above room temperature. Next, formed $Ni(ReO_4)_2$ or $NiO{\cdot}Re_2O_7$ is stable to ca. 890 K. On further heating a drastic change of mass on TG curve is observed. This can be explained assuming that Re_2O_7 is evaporated. According to Material Safety Data Sheet [21] the pure rhenium(VII) oxide melts at 220 °C and boils at 360 °C. It is commonly known that Re_2O_7 sublimes [22]. The most probable mechanism of decomposition is given in section "Analysis of thermal decomposition products". The temperatures, percentage mass of losses and the products of the decomposition of $[Ni(NH_3)_4](ReO_4)_2$ and $[Ni(NH_3)_6](ReO_4)_2$ at particular stages are presented in Tables 2 and 3, respectively. Decomposition of $[Ni(NH_3)_4](ReO_4)_2$ was also a subject of investigations performed by Chakravortiet al. [3]. The measurements were performed up to 573 K. The authors have found that complete deammination takes place in two steps, which is in a good agreement with our results. The intermediate product $[Ni(NH_3)_2](ReO_4)_2$ was characterized using infrared spectroscopy, electronic spectra and magnetic susceptibility measurements [3]. The authors claim that electronic spectra suggest tetragonal symmetry. However, magnetic susceptibility data are characteristic for six coordinated.

We compared our results with those available in the literature for thermal decomposition of the other hexaamminemetal(II) complexes. The first step observed in the following samples: $[Ca(NH_3)_6](ClO_4)_2$, $[Ba(NH_3)_4](ClO_4)_2$ and $[Ni(NH_3)_6]X_2$ (where X = Cl, Br) involving deammination is similar to our results [7, 23, 24]. At the higher temperatures the perchlorates explodes and $CaCl_2$ and $BaCl_2$ are formed as a final product of decomposition. The data presented in [7] suggest that both $[Ni(NH_3)_6]Cl_2$ and $[Ni(NH_3)_6]Br_2$ decompose to Ni as a final product.

Analysis of thermal decomposition products

First, the final product of decomposition was identified. The mass lost registered in TG measurements clearly

Table 1 Comparison of experimental and calculated spectra (DFT, B3LYP6-311 + G(d,p), Lanl2DZ, Lanl2TZ) for $[Ni(NH_3)_6]^{2+}$, $[Ni(NH_3)_4]^{2+}$ and ReO_4^-

IR exper./cm^{-1} $[Ni(NH_3)_6](ReO_4)_2$/$[Ni(NH_3)_4](ReO_4)_2$	$[Ni(NH_3)_6]^{2+}$ +ReO_4^-		$[Ni(NH_3)_4]^{2+}$ +ReO_4^-		Assignment
	Calculated/cm^{-1}	Rel. Intensity/%	Calculated/cm^{-1}	Rel. Intensity/%	
	3,428	20.6	3,409	58.0	
	3,427	0.0	3,407	0.0	
	3,427	0.0	3,403	70.4	
	3,427	21.8	3,402	1.7	
	3,426	21.4	3,397	19.2	ν_{as} NH_3
3,356/3,358	3,426	0.0	3,396	23.2	
	3,425	0.0	3,387	54.8	
	3,425	16.0	3,386	0.0	
	3,425	0.0			
	3,425	15.8			
	3,425	14.9			
	3,424	0.0			
	3,344	0.0	3,326	1.1	
	3,342	8.5	3,321	34.7	
	3,342	8.6	3,318	19.9	ν_{sym} NH_3
3,271/3,270	3,341	0.0	3,317	35.8	
	3,341	9.4			
	3,341	0.0			
	1,650	0.2			
	1,643	0.0			
	1,642	0.0			
	1,631	20.0			
	1,630	6.7	1,628	38.4	
1,616/1,615	1,630	22.8	1,628	30.9	δNH_3
	1,629	0.0	1,625	34.0	
	1,629	0.0	1,619	0.0	
	1,627	0.0	1,619	16.6	
	1,619	27.4	1,612	0.0	
	1,619	30.1	1,610	4.4	
	1,609	0.0	1,608	0.3	
–/1,411	–	–	1,330	0.5	
1,273/1,274	1,303	0.0			
1,255/1,255	1,277	95.4	1,321	100.0	
1,237/1,237	1,276	96.0	1,311	48.4	ωNH_3
1,218/1,220	1,274	100.0	1,308	57.2	
1,191/1,191	1,265	0.0			
	1,265	0.0			
966/966		982			ν_s ReO_4
–/930					
–/924		920			ν_{as} ReO_4
918/916					
913/910					
888/894					
888/889					
676/680	604	0.0	690	55.9	
644/645	603	62.7	686	43.3	

Table 1 continued

IR exper./cm^{-1} $[Ni(NH_3)_6](ReO_4)_2$/$[Ni(NH_3)_4](ReO_4)_2$	$[Ni(NH_3)_6]^{2+}$ + ReO_4^-		$[Ni(NH_3)_4]^{2+}$ + ReO_4^-		Assignment
	Calculated/cm^{-1}	Rel. Intensity/%	Calculated/cm^{-1}	Rel. Intensity/%	
576/580	603	0.0	686	57.3	
	603	0.0	660	0.0	ρNH_3
	603	63.5	632	4.6	
	602	63.5	593	5.7	
	516	0.1	592	0.6	
	514	0.0	585	0.0	
	514	0.0			
	444	0.0			
	443	0.0			
	441	0.0			
–/401	–	–	373	1.3	
–/390	–	–	369	0.1	ν NiN
	–	–	367	0.0	
–/359					
340/345		332			δ_d ReO4
336/336					
326/327	310	0.0	331	0.3	ν NiN
316/317		332			
307/310					δ_d ReO4
	284	0.4			
	282	0.3			ν NiN
232/-	282	0.3			
219/219	216	0.0			ν NiO
	216	0.0			
–/207	–	–			
	182	0.0			
	182	2.1			
	182	2.1			δ_dNNiN
	182	2.1			
	172	0.0			
	170	0.0			
–/150	136	0.0	141	1.9	
	133	0.0	140	3.6	δNNiN
	131	0.0	139	3.2	
–/114			123	0.0	
	95	0.0	93	0.1	
89/92	92	0.0	87	0.0	
73/–	59	0.0	80	0.1	
	47	0.0	74	0.0	$\nu_{L,}$ τNH_3
	36	0.0	41	0.0	
	23	0.0			

suggests that the nickel oxide may be the final decomposition product. The remaining substance after heating the $[Ni(NH_3)_6](ReO_4)_2$ to the ca. 1,275 K was examined after cooling to the room temperature by means of middle (4,000–350 cm^{-1}) and far (600–30 cm^{-1}) infrared spectroscopy. Two separate measurements with appropriate settings of the Bruker VERTEX 70v spectrometer were made for particular IR region. The obtained spectra are shown in Fig. 3a. The MIR and FIR data overlap in the 600–350 wavenumber region. Spectra were normalized

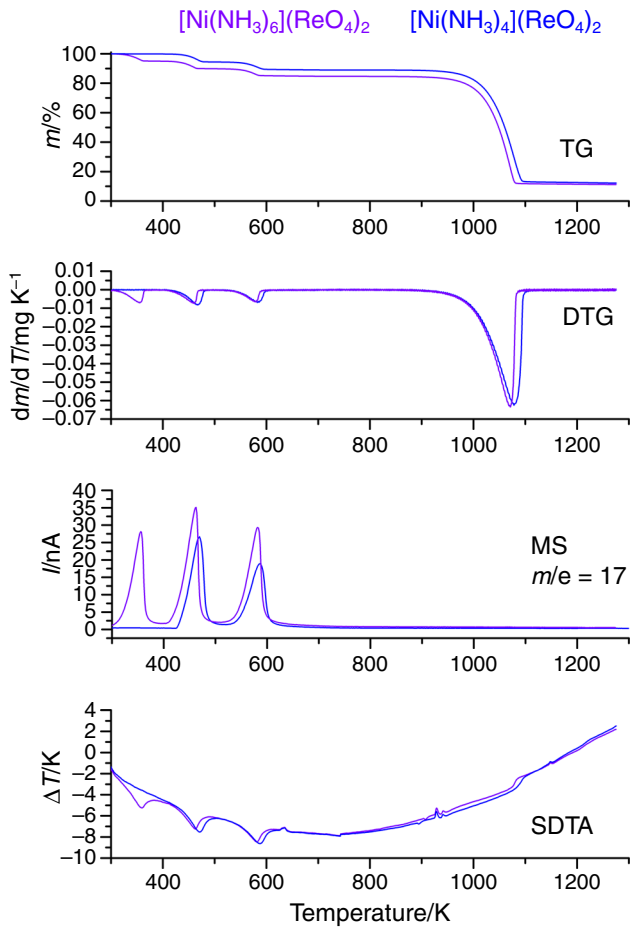

Fig. 2 TG, DTG, SDTA and MS curves for $[Ni(NH_3)_4](ReO_4)_2$ and $[Ni(NH_3)_6](ReO_4)_2$ in the temperature range of 295–1,275 K, at a constant heating rate of 10 K min^{-1}

Table 2 Parameters of $[Ni(NH_3)_4](ReO_4)_2$ thermal analysis

Stage No	Temperature range/K	Mass lost/%	Theoretical mass lost/%	Products of decomposition
1	300–411	0.20		
2	411–483	5.30	5.43	$2NH_3$
3	529–600	5.05	5.43	$2NH_3$
4	890–1,110	76.40	77.23	Re_2O_7
	1,110–1,275	0.85		

Table 3 Parameters of $[Ni(NH_3)_6](ReO_4)_2$ thermal analysis

Stage No	Temperature range/K	Mass loss/%	Theoretical mass loss/%	Products of decomposition
1	300–368	4.90	5.15	$2NH_3$
2	411–470	5.14	5.15	$2NH_3$
3	529–593	4.84	5.15	$2NH_3$
4	890–1,102	73.34	73.25	Re_2O_7
	1,102–1,275	0.54		

(overlapping region was used) to the same intensity and shifted vertically for better visibility. We have compared our results with data available in the literature for nickel oxide. A great similarity between data registered by us and found in Ref. [25–28] can be noticed. Broad and diffused band at ca. 3,410 cm^{-1}, shoulder at 3,219 cm^{-1} and very weak at ca. 1,628 cm^{-1} can be assigned to water O–H stretching vibrations and H–O–H bending vibration, respectively [10]. The presence of these bands is caused by absorption of water from the air during preparing sample pellet in KBr. The traces of Re_2O_7 remained in the sample are probably responsible for the band at 910 cm^{-1}. In case of samples containing ReO_4^- anion, this band is very intensive in IR measurements. The most intense and broad band with maximum at 406 cm^{-1} can be assigned to Ni–O vibrations. One should notice an excellent agreement between MIR and FIR spectra in the overlapping region. However, the FT-FIR measurements reveal more detail. Three, well-separated components at 571 (shoulder), 492, and 406 cm^{-1} are readily visible, whereas in the FT-MIR spectrum rather one broad maximum with shoulders is present. This is probably due to different detectors used. Below 400 cm^{-1} none bands appear. A question has arisen what product remains after complete deammination but before the last step of decomposition? One can assume that the $[Ni(NH_3)_6]^{2+}$ simply loses NH_3 ligands, and the $Ni(ReO_4)_2$ is formed in which Ni^{2+} and ReO_4^- ions exists separately in the crystal structure. The crystal structure of $Ni(ReO_4)_2$ was reported by Butz et al. [29]. The Ni atom is surrounded by six oxygen atoms. The formed octahedron is fairly regular. Three of the oxygen atoms belonging to each ReO_4^- anion are engaged in formation of the bonds (so called bridge bond) to Ni, whereas one oxygen (so called terminate) atom is bound only to Re. Each ReO_4 unit links three cation octahedra. The Ni–O distance is equal to 1.976 Å and is slightly shorter than observed in pure NiO (2.096 Å). Anion is distorted. One Re–O bond is longer (1.976 Å) in comparison with the three remaining (1.789 Å). The structure is built from layers consisting of octahedra linked by anion tetrahedra. In order to check the intermediate product, the second thermogravimetric measurement was run. A $[Ni(NH_3)_6](ReO_4)_2$ sample of mass equal to 31.7,521 mg was heated from 298 to 748 K and next cooled to room temperature. The final mass lost registered on TG curve was equal to 14.6 % which well corresponds to theoretical value for six ligands lost. The remaining, so called intermediate product was examined using FT-FIR and FT-MIR spectroscopy. Figure 3b presents obtained spectra. In the MIR region, five main bands are clearly visible. The strong, broad band at ca. 3,388 cm^{-1} and shoulder at 3,226 cm^{-1} can be assigned to both NH_3 and H_2O stretching vibrations. The former possibility should be rather excluded from our consideration for the following reasons. Firstly, TG measurements clearly showed that NH_3

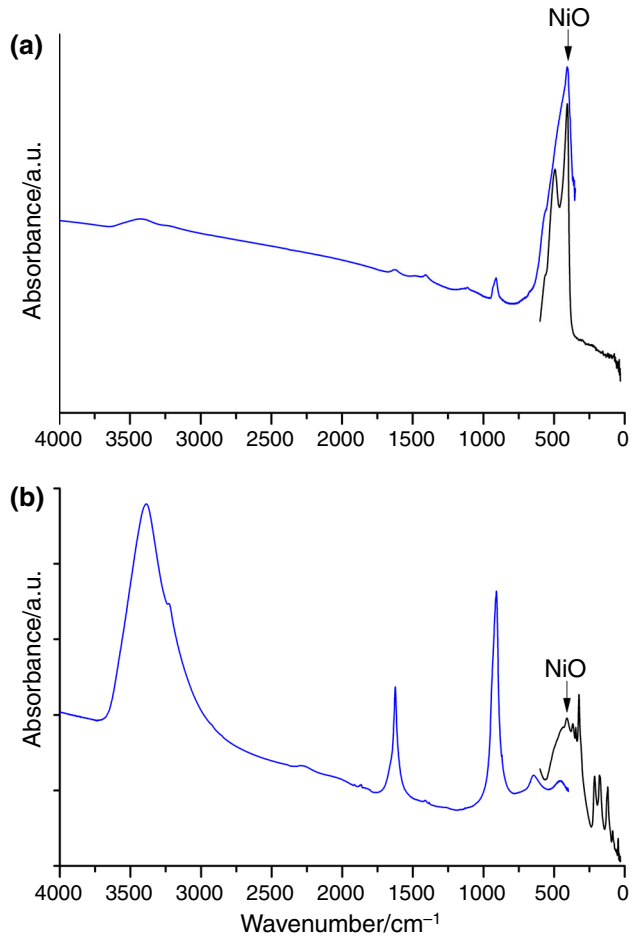

Fig. 3 FT-MIR and FT-FIR spectra of **a** final and **b** intermediate decomposition products

ligands were almost completely removed from the sample. Even if we assume that deammination was not complete and some small amount remained in the investigated sample, the resulting spectrum should show much less intense band than it is observed experimentally. Secondly, the position of these bands corresponds well with those visible in Fig. 3a. The shape and its broadening also recalls bands observed in the compounds containing O–H stretching vibrations. Moreover, these bands are shifted toward lower wavenumbers (by ca. 30 cm^{-1}) with respect to NH_3 stretching vibrations bands registered for $[Ni(NH_3)_6](ReO_4)_2$ and $[Ni(NH_3)_4](ReO_4)_2$. Thirdly, when the dry sample was prepared for IR transparent measurements (KBr was also dried for 4 days at 470 °C), we have noticed that it becomes sticky. The last indicates that intermediate product of decomposition is very hygroscopic. The H–O–H bending vibration is responsible for a band visible at 1,624 cm^{-1}. Next strong band at 908 cm^{-1} is associated with ν_3 antisymmetric ReO_4^- vibration [10]. Two weak and broad bands at 639 and 457 cm^{-1} are connected with rocking H_2O vibrations.

Table 4 Comparison of Re_2O_7 wavenumbers obtained by different authors in the 500–30 cm^{-1} with data registered for $Ni(ReO_4)_2$ and $[Ni(NH_3)_4](ReO_4)_2$

This work $Ni(ReO_4)_2$/ $[Ni(NH_3)_4](ReO_4)_2$ wavenumber/cm^{-1}	Ref [29] wavenumber/ cm^{-1}	Ref [30] wavenumber/ cm^{-1}	Ref [31] wavenumber/ cm^{-1}
		384	
368/359		372	
		352	
347/345	345 (IR)	339	342
–/336	342 (RS)		
324/327			
–/317	305 (IR)	302	
–/310		296	
		258	
213/219		216	
178/–	174 (RS)	166	170
–/150		150	
120/114		116	
85/92		97	
	61 (RS)	63	
		51	
46		45	

The FIR region is rich in bands. The first band at 457 cm^{-1} covers the same region as MIR. Next at 409 cm^{-1} comes from the Ni–O (compare Fig. 3a). Three bands located at 368, 347, 324 cm^{-1}) are associated with vibrations in ReO_4^-. As was stated in the section "Spectroscopic identification of samples," the regular ReO_4^- has the following vibrations: $\nu_1(A_1) \approx 971\ cm^{-1}$, $\nu_2(E) \approx 331\ cm^{-1}$, $\nu_3(T_2) \approx 920\ cm^{-1}$, and $\nu_4(T_2) \approx 331\ cm^{-1}$ but only T_2 are IR active. However, when the symmetry is disturbed the selection rules are broken and splitting and shifting of the particular bands can occur. It is interesting to notice that the remaining frequencies (at 213, 178, 120, 85, 46 cm^{-1}) agree well with those reported in the literature for solid state of Re_2O_7 and acquired by Raman spectroscopy [30–32]. The comparison of frequencies obtained in this work and in Ref [30–32] is given in Table 4. The Re_2O_7 compound consists of ReO_4 tetrahedral and distorted ReO_6 octahedral units which are connected through corners to form polymeric chain [14]. The evidence of Ni–O bond formation is also clearly visible. The similar behaviour was found in $Ni(ClO_4)_2$ [10, 33]. Strong interaction between Ni^{2+} and ClO_4^- exists and as a result bridging tridentate bonds are formed. Pascal et al. suggests the octahedral environment around the metal atom, and a polymeric structure [33, 34].

Phase transition

Figure 4 shows the temperature dependencies of the heat flow (DSC curves) obtained on heating (lower, red curves)

and on cooling (upper, blue curves) of the $[Ni(NH_3)_4](ReO_4)_2$ (denoted as 1) and of the $[Ni(NH_3)_6](ReO_4)_2$ (denoted as 2) samples with scanning rate 10 K min^{-1}. In the same figure additional curves in a limited temperature range registered on heating for $[Ni(NH_3)_4](ReO_4)_2$ are also presented. These curves were obtained in the second run of DSC measurements (scanning rate = 10, 20 K min^{-1}). One can see in Fig. 4 that in the temperature range 140–300 K $[Ni(NH_3)_4](ReO_4)_2$ possesses phase transition in solid state. One very small, diffused anomaly on each of appropriate DSC curves was registered at $T^{h}_{Cpeak} = 187.8$ K (on heating) and at $T^{c}_{Cpeak} = 185.3$ K (on cooling). Small hysteresis and the λ shape of this phase transition suggest the second-order type phase transition. The thermodynamic parameters of the detected phase transition obtained during heating are presented in Table 5. On cooling at different rates this anomaly becomes very broad and diffused and hence determination of phase transition parameters is impossible. In contradiction to $[Ni(NH_3)_4](ReO_4)_2$ the $[Ni(NH_3)_6](ReO_4)_2$ does not have any phase transition in the temperature range of 300–140 K. This is rather unusual behaviour because hexaamminenickel(II) complexes with different anions (Cl^-, Br^-, ClO_4^-, BF_4^- NO_3^-) exhibit rich polymorphism. Moreover, these compounds are rather stable even in air. The phase transitions temperatures detected for compounds containing simple anions are the lowest in the series [2 and papers cited therein]. As one could expected exchanging simple anion to the tetrahedral one cause that phase transition are observed at higher temperatures [1, 2]. We expected that in the case of hexaamminenickel(II) perrhenate the situation will be analogical i.e. one or two phase transitions will be found at even higher temperatures.

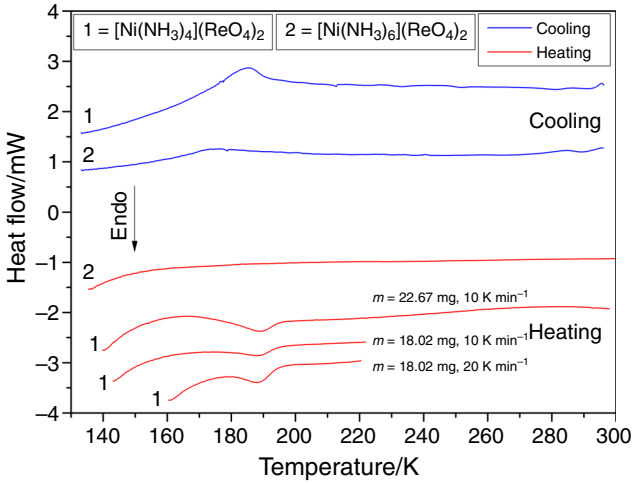

Fig. 4 DSC curves registered on heating and cooling of $[Ni(NH_3)_4](ReO_4)_2$ and $[Ni(NH_3)_6](ReO_4)_2$ samples in the temperature range of 140–300 K at a rate of 10 K min^{-1}

Table 5 Thermodynamic parameters of the phase transitions of $[Ni(NH_3)_4](ReO_4)_2$

	Heating	Cooling
T_c/K	187.8 ± 0.1	185.0 ± 0.1
$\Delta H \pm \delta\Delta H$/J mol^{-1}	307.0 ± 80.0	
$\Delta S \pm \delta\Delta S$/J $mol^{-1}K^{-1}$	1.6 ± 0.4	

Calculation of the activation energy by isoconversional methods

In this work we have used KAS model-free approach and Kissinger method for determination of activation energy for the decomposition steps. The model-free methods employed in this work are based on dynamic TG/DTG analysis and they are recommended by ICTAC Kinetics Committee. Moreover, the KAS method provides more accurate results for solid-state reactions [35]. The theoretical background of non-isothermal kinetics of condensed phase reactions can be found in the most papers [36–39].

The KAS model-free method that can be obtained by applying the following approximation [4, 5]:

$$\ln\left(\frac{\beta}{T_{\alpha}^2}\right)_i = \ln\left(\frac{R \cdot A}{E_{a,\alpha} \cdot g(\alpha)}\right) - \frac{E_{a,\alpha}}{R} \cdot \frac{1}{T_{\alpha,i}} \quad (1)$$

where: i is the number of experiment, β is the linear heating rate, $E_{a,\alpha}$ is the activation energy corresponding to conversion α, and R is the gas constant, A is the Arrhenius frequency factor, $g(\alpha)$ is the mechanism function, $T_{\alpha,i}$ is the temperature at a given conversion α for the experiment i.

The method is based on measurements of temperatures for each conversion degree α and different heating rates β. The plots of $\ln\left(\frac{\beta}{T_{\alpha}^2}\right)$ versus $1/T_{\alpha}$ at constant α will give straight line and from the slope $-\frac{E_a}{R}$, activation energies are determined.

Kissinger equation [5] which yields a single value of activation energy was also used to determine the activation energy.

$$\ln\left(\frac{\beta}{T_{max}^2}\right)_i = \text{Const.} - \frac{E_a}{R} \cdot \frac{1}{T_{max,i}} \quad (2)$$

where: T_{max} is the temperature of peak maximum from the DTG graph.

A plot of $\ln\left(\frac{\beta}{T_{\alpha}^2}\right)$ against $1/T_{max}$ gives the Arrhenius plot from the slope of which activation energy can be determined.

The kinetic parameters obtained by KAS method for all decomposition steps were calculated according to Eq. (1) for a given value of conversion α. In the present study, three different heating rates were used (5, 7.5 and

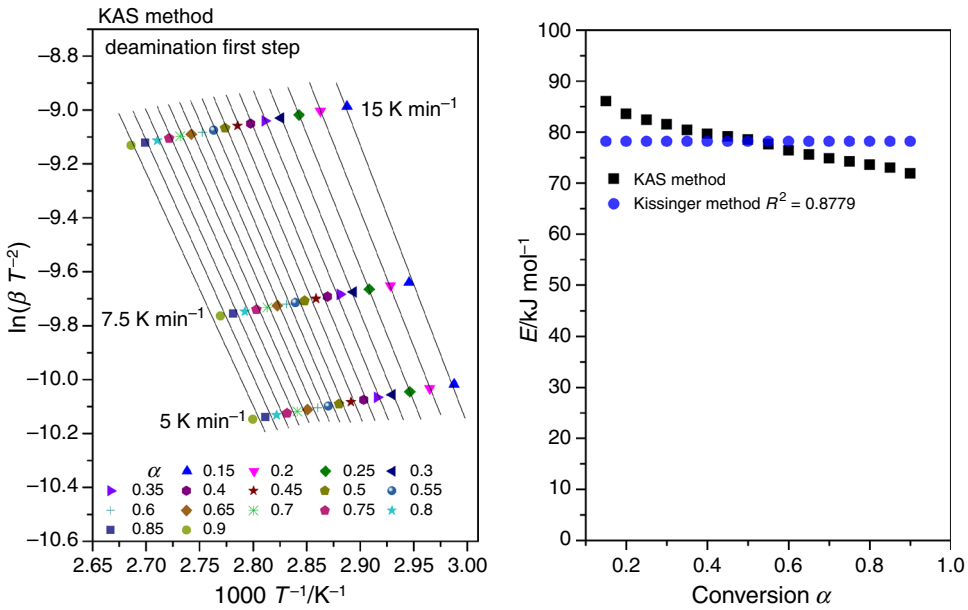

Fig. 5 Application of KAS kinetic method and isoconversional activation energy for first step of deammination process of $[Ni(NH_3)_6](ReO_4)_2$ at each extent of conversion (α from 0.15 to 0.9)

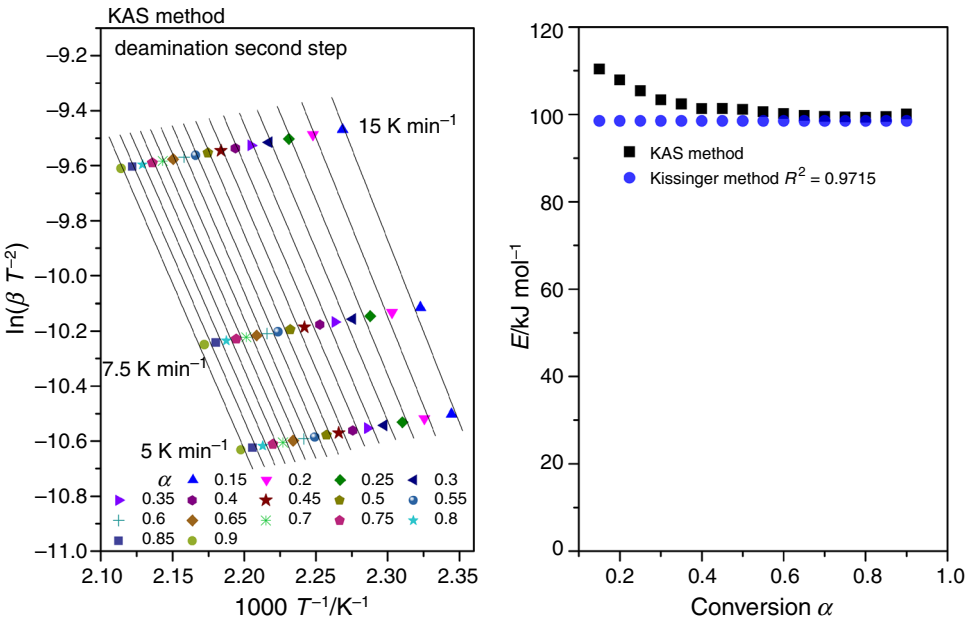

Fig. 6 Application of KAS kinetic method and isoconversional activation energy for second step of deammination process of $[Ni(NH_3)_6](ReO_4)_2$ at each extent of conversion (α from 0.15 to 0.9)

15 K min^{-1}). The calculation procedures of Kissinger equation were applied according to Eq. 2.

The corresponding lines of KAS method obtained at different conversion degrees (α from 0.15 to 0.9) and different heating rates β for first step of deammination process of $[Ni(NH_3)_6](ReO_4)_2$ are shown in Fig. 5, where the analogous lines of the remaining stages were obtained with the same methodology (see Figs. 6–8).

The apparent activation energies of $[Ni(NH_3)_6](ReO_4)_2$ for all stages of decomposition were calculated using KAS and Kissinger methods and are shown in Figs. 5–8. In Table 6, the R^2 parameters of the fit and activation energy values E by KAS method for all the steps of decomposition.

From the dependence of activation energy on the extent of conversion, we can predict the nature of solid-state reactions. If E_a values are independent of α, the decomposition process is dominated by a single step reaction [40, 41]; on the contrary, a significant variation of E_a with α should be interpreted in terms of multi-step mechanism [42, 43]. As we can see in Fig. 5 for the first step of deammination of $[Ni(NH_3)_6](ReO_4)_2$, the activation energy calculated by KAS method slightly decreases with conversion (α from 0.15 to 0.9). This behaviour indicates that

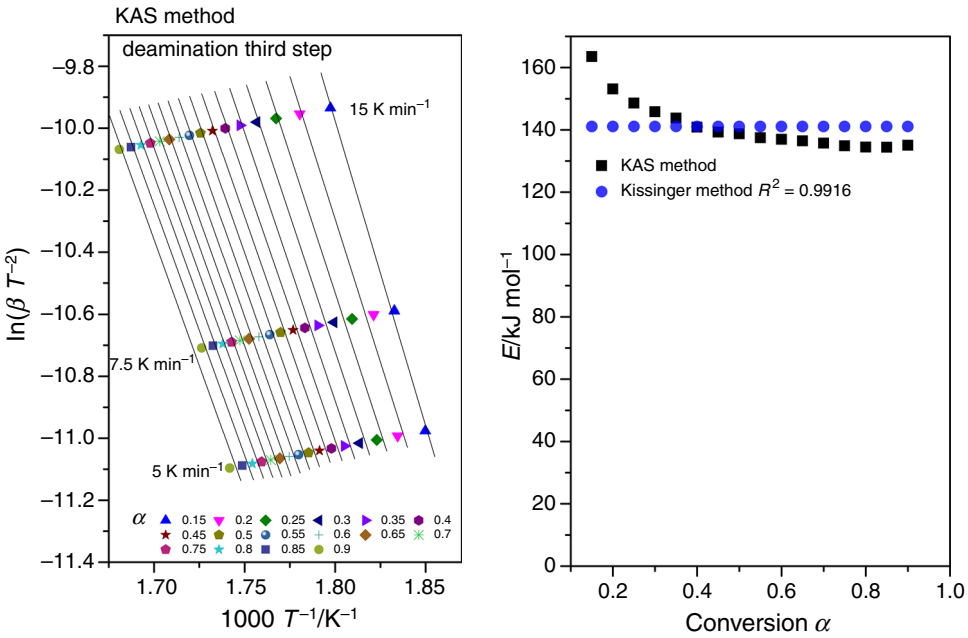

Fig. 7 Application of KAS kinetic method and isoconversional activation energy for third step of deammination process of $[Ni(NH_3)_6](ReO_4)_2$ at each extent of conversion (α from 0.15 to 0.9)

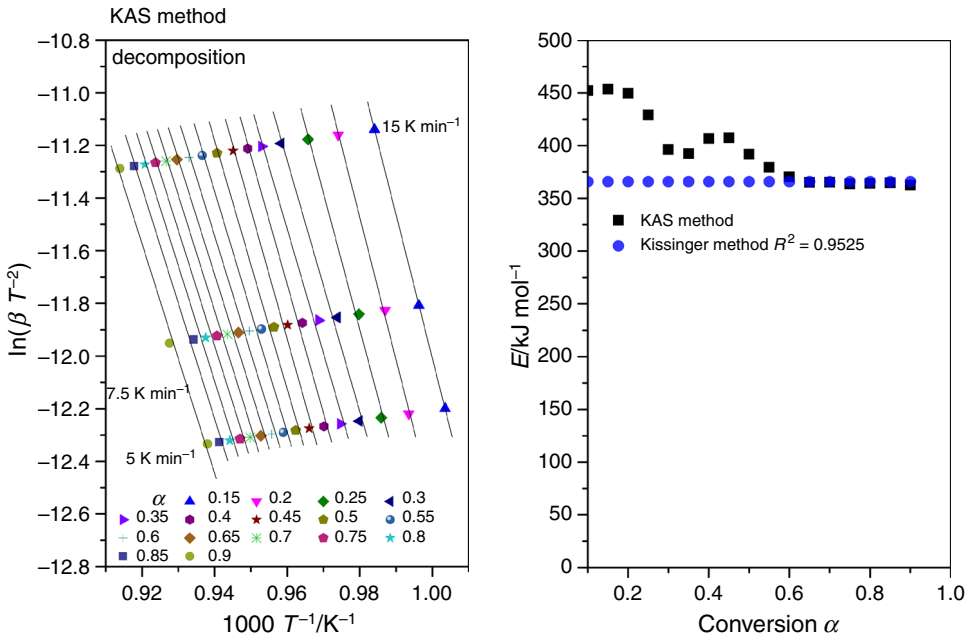

Fig. 8 Application of KAS kinetic method and isoconversional activation energy for decomposition process of $[Ni(NH_3)_6](ReO_4)_2$ at each extent of conversion (α from 0.15 to 0.9)

probably only one mechanism is involved for the first step of deammination. The mean value for the activation energy obtained from the KAS method is $E_{a(KAS)} = 76.66 \pm 3.07$ kJ mol^{-1} and from the Kissinger method is $E_{a(KIS)} = 78.21 \pm 18.60$ kJ mol^{-1}.

The activation energy of the second and third steps of deammination process of $[Ni(NH_3)_6](ReO_4)_2]$ is almost constant for α between 0.3 and 0.9 (see Figs. 6, 7). This behaviour suggests that this process is simple and can be described by a single reaction. The mean values of the activation energy corresponding to the second and third stages of deammination are: $E_{a(KAS)} = 100.62 \pm 1.24$ kJ mol^{-1} and $E_{a(KIS)} = 98.52 \pm 11.72$ kJ mol^{-1} (the second stage) and $E_{a(KAS)} = 137.99 \pm 3.62$ kJ mol^{-1} and $E_{a(KIS)} = 141.09 \pm 12.30$ kJ mol^{-1} (the third stage). The data show that energy of activation was found to be independent of conversion degrees (α from 0.3 to 0.9). The values of activation energy obtained from the Kissinger method are consistent with the range of values obtained by the KAS method and are very near to their average values.

Chakravorti et al. [3] investigated deammination of the $[Ni(NH_3)_4](ReO_4)_2$ compound. They were able to

Table 6 The activation energy values E at $\beta = 5$, 7.5, and 15 K min^{-1} by KAS method

α	Deammination first step		Deammination second step		Deammination third step		Decomposition	
	E/kJ mol^{-1}	R^2	E/kJ mol^{-1}	R^2	E/kJ mol^{-1}	R^2	E/kJ mol^{-1}	R^2
KAS method								
0.15	86.1	0.995	110.4	0.980	163.5	0.995	453.5	0.999
0.2	83.6	0.952	107.9	0.983	153.1	0.959	449.7	0.997
0.25	82.4	0.992	105.4	0.979	148.6	0.958	429.1	0.989
0.3	81.5	0.999	103.4	0.974	145.8	0.961	396.4	0.979
0.35	80.4	0.999	102.4	0.976	143.8	0.963	392.3	0.976
0.4	79.7	0.998	101.3	0.978	140.9	0.962	406.8	0.980
0.45	79.1	0.996	101.3	0.983	139.3	0.959	407.4	0.980
0.5	78.5	0.993	101.1	0.988	138.7	0.967	391.8	0.977
0.55	77.6	0.989	100.6	0.989	137.5	0.970	379.4	0.974
0.6	76.4	0.987	100.2	0.989	136.9	0.975	370.2	0.972
0.65	75.6	0.981	99.8	0.988	136.5	0.978	365.2	0.972
0.7	74.8	0.972	99.6	0.988	135.7	0.976	365.3	0.975
0.75	74.2	0.967	99.4	0.988	134.9	0.972	363.7	0.975
0.8	73.6	0.964	99.4	0.987	134.5	0.969	364.2	0.981
0.85	73.0	0.967	99.5	0.988	134.4	0.968	364.7	0.988
0.9	71.9	0.970	100.1	0.989	135.0	0.962	362.4	0.988

determine activation energy but only for the last step, i.e., $[Ni(NH_3)_2](ReO_4)_2 \rightarrow Ni(ReO_4)_2$. The Ea value obtained by these authors equals to 97 kJ mol^{-1} and is lower than obtained by us. We have used three independent TG measurements (according to ICTAC Kinetics Committee recommendation) in order to estimate the Ea instead of only one. Moreover, one can see that linear fit obtained in Ref [3] is not very good and hence the estimated value of Ea is associated with larger error.

For the last decomposition stage (Fig. 8), the activation energy fluctuates with α increasing (degree of conversion α from 0.15 to 0.5). This means that the reaction mechanism is not the same as in the decomposition process and that activation energy is dependent on conversion degrees (α from 0.15 to 0.5). On conversion degrees α from 0.5 to 0.9, the activation energy remains practically constant, with the average values of $E_{a(KAS)} = 369.66 \pm 9.78$ kJ mol^{-1} calculated using the KAS method. Activation energy calculated by Kissinger method equal to 365.86 ± 48.22 kJ mol^{-1}. As one could expect the energy activation for the first step of deammination is the lowest. This fully confirms that 2 of 6 NH_3 ligands in $[Ni(NH_3)_6](ReO_4)_2$ are weaker bonded.

Conclusions

1. One phase transition at ca. $T_c^h = 188$ K (on heating) and $T_c^c = 185$ K (on cooling) in $[Ni(NH_3)_4](ReO_4)_2$ was detected by means of differential scanning calorimetry in the temperature range 300–140 K. The λ shape of the anomaly suggests the second-order phase transition. The $[Ni(NH_3)_6](ReO_4)_2$ does not exhibit any phase transition in this region.
2. Decomposition of both compounds can be divided into two main steps. The first step connected with the deammination can be further divided into three or two sub-steps for $[Ni(NH_3)_6](ReO_4)_2$ and $[Ni(NH_3)_4](ReO_4)_2$, respectively. It is completed up to ca. 600 K. In the second step, the Re_2O_7 is released above ca. 900 K and NiO is formed as a final product.
3. The FT-MIR spectra of both compounds are very similar, however, in case of $[Ni(NH_3)_4](ReO_4)_2$ a weak band at ca. 1,411 cm^{-1} appears. Infrared spectra calculated by the DFT method (Gaussian09 B3LYP, 6-311 + G(d,p), Lanl2DZ, Lanl3TZ) for isolated $[Ni(NH_3)_4]^{2+}$, $[Ni(NH_3)_6]^{2+}$ cations, and ReO_4^- anion are in a good agreement with respective experimental data.
4. The FT-FIR data revealed that ReO_4^- anions situation is different in both discussed compounds. In the $[Ni(NH_3)_6](ReO_4)_2$, these anions have disturbed tetrahedral symmetry. In the case of $[Ni(NH_3)_4](ReO_4)_2$, some additional bands can be interpreted as an evidence of forming polymeric chains by ReO_4 units.
5. The activation energy for particular steps was determined for $[Ni(NH_3)_6](ReO_4)_2$ using Kissinger–

Akahira–Sunose model-free approach and Kissinger method. The lowest value was obtained for the first step of deammination. The activation energies calculated for the deammination steps of $[Ni(NH_3)_6](ReO_4)_2$ by this two methods were found to be consistent and indicate that only one mechanism is involved for the decomposition.

Acknowledgements Our thanks are due to Professors A. Migdał-Mikuli and E. Mikuli for stimulating discussions. The research (FT-IR) was carried out with the equipment purchased thanks to the financial support of the European Regional Development Fund in the framework of the Polish Innovation Economy Operational Program (contract no. POIG.02.01.00-12-023/08).This research was supported in part by PL-Grid Infrastructure. The project was supported by grant of the Polish Plenipotentiary to JINR and JINR Directorate from 26.04.2012, Nr 235 p.9.

References

1. Rachwalska M, Janik JM, Janik JA, Pytasz G, Waluga T. Specific heat of solid $[Ni(NH_3)_6]$ $(ClO_4)_2$ in the temperature range from 115 to 300 K. Phys Stat Sol (a). 1975;30:K81–2.
2. Grzybek T, Janik JA, Mayer J, Pytasz G, Rachwalska M, Waluga T. Specific heat and phase transition in $[Ni(NH_3)_6]BF_4)_2$. Phys Stat Sol (a). 1973;16:K165–6.
3. Chakravorti MC, Sarkar MB, Bharadwaj PK. Rhenium part XV. Tetragonal complexes of Nickel(II) containing coordinated perrhenate $[ReO_4]^-$. Transit Met Chem. 1981;6:211–4.
4. Akahira T, Sunose T. Method of determining activation deterioration constant of electrical insulating materials. Res Report Chiba Inst Technol (SciTechnol). 1971;16:22–31.
5. Kissinger HE. Variation of peak temperature with heating rate in differential thermal analysis. J Res Natl Bur Stand. 1956;57:217–21.
6. Kissinger HE. Reaction kinetics in differential thermal analysis. Anal Chem. 1957;29:1702–6.
7. Rejitha KS, Ichikawa T, Mathew S. Thermal decomposition studies of $[Ni(NH_3)_6]X_2$ (X = Cl, Br) in the solid state using TG-MS and TR-XRD. J Therm Anal Calorim. 2011;103:515–23.
8. Briscoe HVA, Robinson PL, Rudge AJ. The perrhenates of copper, nickel and cobalt. J Chem Soc. 1931:2211–13; doi:10.1039/JR9310002211.
9. Pitzer KS. The crystal structure of tetraamminecadmium perrhenate, $[Cd(NH_3)_4](ReO_4)_2$. Z Krist Krist Krist Krist. 1935;92:131–5.
10. Nakamoto K. Infrared and Raman spectra of inorganic and coordination compounds, part B:applications in coordination, organometallic, and bioinorganic chemistry. 6th ed. Hoboken: John Wiley & Sons; 2009.
11. Migdał-Mikuli A, Mikuli E, Barańska M, Hetmańczyk Ł. Vibrational spectrum and molecular structure of $[Cu(NH_3)_5](ClO_4)_2$. ChemPhysLett. 2003;381:329–34.
12. Mikuli E, Hetmańczyk Ł, Medycki W, Kowalska A. Phase transitions and molecular motions in $[Zn(NH_3)_4](BF_4)_2$ studied by nuclear magnetic resonance, infrared and Raman spectroscopy. J Phys Chem Solids. 2007;68:96–103.
13. Müller A, Böschen I, Baran EJ. Über Hexamminmetallchalkogenometallat. Monatsh Chem. 1973;104:821–35.
14. Krebs B, Muller A, Beyer HH. The crystal structure of rhenium(VII) oxide. Inorg Chem. 1969;8:436–43.
15. Frisch J, Trucks GW, Schlegel HB, Scuseria GE, Robb MA, Cheeseman JR, Scalmani G, Barone V, Mennucci B, Petersson GA, Nakatsuji H, Caricato M, Li X, Hratchian HP, Izmaylov AF, Bloino J, Zheng G, Sonnenberg JL, Hada M, Ehara M, Toyota K, Fukuda R, Hasegawa J, Ishida M, Nakajima T, Honda Y, Kitao O, Nakai H, Vreven T, Montgomery JA Jr, Peralta JE, Ogliaro F, Bearpark M, Heyd JJ, Brothers E, Kudin KN, Staroverov VN, Keith T, Kobayashi R, Normand J, Raghavachari K, Rendell A, Burant JC, Iyengar SS, Tomasi J, Cossi M, Rega N, Millam JM, Klene M, Knox JE, Cross JB, Bakken V, Adamo C, Jaramillo J, Gomperts R, Stratmann RE, Yazyev O, Austin AJ, Cammi R, Pomelli C, Ochterski JW, Martin RL, Morokuma K, Zakrzewski VG, Voth GA, Salvador P, Dannenberg JJ, Dapprich S, Daniels AD, Farkas O, Foresman JB, Ortiz JV, Cioslowski J, Fox DJ. Gaussian 09, Revision C.01M. Gaussian, Inc., Wallingford CT, 2010.
16. Becke AD. Density-functional thermochemistry. III. The role of exact exchange. J Chem Phys. 1983;98:5648–52.
17. Stephens PJ, Devlin FJ, Chabalowski CF, Frisch MJ. Ab initio calculation of vibrational absorption and circular dichroism spectra using density functional force fields. J Phys Chem. 1994;98:11623–7.
18. Roy LE, Hay PJ, Martin RL. Revised basis sets for the LANL effective core potentials. J Chem Theory Comput. 2008;4:1029–31.
19. Schuchardt KT, Didier BT, Elsethagen T, Sun L, Gurumoorthi V, Chase J, Li J, Windus TL. Basis set exchange: a community database for computational sciences. J ChemInf Model. 2007;47:1045–52.
20. Merrick JP, Moran D, Radom L. An evaluation of harmonic vibrational frequency scale factors. J Phys Chem. 2007;111:11683–700.
21. Sigma-Aldrich Material Safety Data Sheet Rhenium(VII) oxide http://www.sigmaaldrich.com/MSDS/MSDS/DisplayMSDSPage.do?country=US&language=en&productNumber=515736&brand=ALDRICH&PageToGoToURL=http%3A%2F%2Fwww.sigmaaldrich.com%2Fcatalog%2Fsearch%3Finterface%3DAll%26term%3Drhenium%2Boxide%26lang%3Den%26region%3DUS%26focus%3Dproduct%26N%3D0%2B220003048%2B219853269%2B219853286%26mode%3Dmatch%2520partialmax Material Safety Data Sheet. Accessed 21 Jan 2014.
22. Lacheen HS, Cordeiro PJ, Iglesia E. Structure and catalytic function of re-oxo species grafted onto H-MFI zeolite by sublimation of Re_2O_7. J Am Chem Soc. 2006;128:15082–3.
23. Migdał-Mikuli A, Hetmańczyk J. Thermal behavior of $[Ca(H_2O)_4](ClO_4)_2$ and $[Ca(NH_3)_6](ClO_4)_2$. J Thermal Anal Calorim. 2008;91:529–34.
24. Migdał-Mikuli A, Hetmańczyk J, Mikuli E, Hetmańczyk Ł. Thermal behaviour of polycrystalline $[Ba(H_2O)_3](ClO_4)_2$ and $[Ba(NH_3)_4](ClO_4)_2$. Thermochim Acta. 2009;487:43–8.
25. HongxiaQiao, Zhiqiang Wei, Hua Yang, Lin Zhu, and Xiaoyan Yan. Preparation and characterization of NiO nanoparticles by anodic arc plasma method. J Nanomater. 2009. doi:10.1155/2009/795928; Article ID 795928.
26. Biju V, Abdul Khadar M. Fourier transform infrared spectroscopy study of nanostructured nickel oxide. Spectrochimica Acta Part A. 2003;59:121–34.
27. Kashani Motlagh MM, Youzbashi AA, Sabaghzadeh L. Synthesis and characterization of Nickel hydroxide/oxide nanoparticles by the complexation-precipitation. Method Int J Phys Sci. 2011;6:1471–76, doi:10.5897/IJPS11.025.
28. Dulina I, Klochkov L, Danilenko M, Ragulya A. Synthesis of Ni/NiO nanopowder by thermal decomposition of nickel acetate amine. In: Proceedings of the international conference nanomaterials: applications and propeRTIES. 2012;1; 01PCN11(3 pp).

29. Butz A, Miehe G, Paulus H, Strauss P, Fuess H. The crystal structures of $Mn(ReO_4)_2{\cdot}2H_2O$ and of the anhydrous perrhenates $M(ReO_4)_2$ of divalent manganese, cobalt, nickel, and zinc. J Solid State Chem. 1998;138:232–7.
30. Beattie IR, Gilson TR, Jones PJ. Vapor phase vibrational spectra for Re_2O_7 and the infrared spectrum of gaseous $HReO_4$ molecular shapes of Mn_2O_7, Tc_2O_7, and Re_2O_7. Inorg Chem. 1996;35: 1301–4.
31. Beattie IR, Ozin GA. Vibrational spectrum of gaseous, liquid, and solid Re_2O_7. J Chem Soc (A). 1969:2615–19, doi:10.1039/J19690002615.
32. Cunin F, Favier F, Pascal JL. The bridging bidentateperchlorato group in ReO3(ClO4), ReO3(ClO4)Cl2O6 and Sb2Cl6(O)(OH)(ClO4), a vibrational analysis. Spectrochimica Acta Part A. 2002;58:2869–75.
33. Pascal JL, Potier J, Zhang CS. Chlorine trioxide, Cl_2O_6, a most efficient perchlorating reagent in new syntheses of anhydrous metal perchlorates, chloryl and nitryl perchloratometalates of cobalt(II), nickel(II), and copper(II). Reactivity of chlorine trioxide with anhydrous or hydrated chlorides and nitrates. J ChemSoc Dalton Trans. 1985: 297–305.
34. Pascal JL, Potier J, Jones DJ, Roziere J, Michalowicz A. Structural approach to the behavior of perchlorate as a ligand in transition-metal complexes using EXAFS, IR, and Raman spectroscopy. 2. Crystal structure of $M(ClO_4)_2$ (M=Co, Ni). A novel mode of perchlorate coordination. Inorg Chem. 1985;24:238–41.
35. Vyazovkin S, Burnham AK, Criado JM, Perez-Maqueda LA, Popescu C, Sbirrazzuoli N. ICTAC kinetics committee recommendations for performing kinetic computations on thermal analysis data. Thermochim Acta. 2011;520:1–19.
36. Brown ME, Dollimore D, Galwey AK. Reactions in the solid state. Comprehensive chemical kinetics, vol. 22. Amsterdam: Elsevier; 1980.
37. Vyazovkin S, Wight CA. Kinetics in solids. Annu Rev Phys Chem. 1997;48:125–49.
38. Boonchom B. Kinetic and thermodynamic studies of $MgHPO_4.3H_2O$ by non-isothermal decomposition data. J Therm Anal Calorim. 2009;98:863–71.
39. Rotaru A. Thermal analysis and kinetic study of Petrosani bituminous coal from Romania in comparison with a sample of Ural bituminous coal. J Therm Anal Calorim. 2012;110:1283–91.
40. Vyazovkin S. Computational aspects of kinetic analysis.: Part C. The ICTAC Kinetics Project—the light at the end of the tunnel? Thermochim Acta. 2000;355:155–63.
41. Boonchom B. Kinetics and thermodynamic properties of the thermal decomposition of manganese dihydrogen phosphate dihydrate. J ChemEng Data. 2008;53:1533–8.
42. Yu He, Sen Liao, Zhipeng Chen, Qian Chai, Yu Li, Yaoyi Su, Wenwei Wu, Bin Li. Application of isoconversional calculation procedure to non-isothermal kinetics study Part II. Thermal decomposition of $NH_4CuPO_4{\cdot}H_2O$. J Therm Anal Calorim. 2013;111:313–21.
43. Vyazovkin S. Nicolas Sbirrazzuoli N. Isoconversional method to explore the mechanism and kinetics of multi-step epoxy cures. Macromol Rapid Commun. 1999;20:387–9.